Seventh International Conference on Computational Fluid Dynamics (ICCFD7), Big Island, Hawaii, July 9-13, 2012 **ICCFD7-2703**

LES Study on Vortex Ring-Shock Interaction behind MVG

Yonghua Yan*, Xiao Wang*, Caixia Chen* and Chaoqun Liu *,**

* University of Texas at Arlington, USA.
** University of Texas at Arlington, USA.

Abstract: The interaction of vortex rings and oblique shocks, generated by the micro vortex generator (MVG) controlled ramp flow at M = 2.5 and Re_θ =5760, is studied by implicit large eddy simulation (LES) with the 5th order Bandwidth-optimized WENO scheme. A turbulent inflow was generated by a separate DNS for boundary layer transition. It shows that the vortex ring structure generated by MVG is very stable, does not break down and keeps it original topology after penetrating the strong shock wave. However, the oblique shocks are broken when they interact with the vortex rings. The bump on the 3D shock wave surface is observed. The separation zone, which is originally generated by the shock-boundary layer interaction, is significantly reduced due to the vortex ring-shock interaction.

Keywords: Shock, Vortex Ring, MVG, Turbulence.

1 Introduction

In the supersonic ramp jets, shock boundary layer interaction (SBLI) can significantly reduce the quality of the flow field by triggering large-scale separation, causing total pressure loss, making the flow unsteady and distorting. Micro vortex generators (MVG) are a kind of low-profile passive control device designed for the boundary layer control. In contrast to the conventional VG (widely used in aviation applications and with height (h) of the order of the boundary-layer(δ), micro VG has a height approximately 20-40% (more or less) of the boundary layer. Among these micro VGs, mircoramp vortex generators (MVG) are given special interest by engineers because of their structural robustness. MVG generates a pair of streamwise vortex, which remains in the in the boundary layer for relatively long distance, and the corresponding "down-wash" effect will bring momentum exchange to the boundary layer which makes it less liable to be separated. During such process, a specific phenomenon called "momentum deficit", i.e., a cylindrical region consisted of low speed flows, will be formed after the MVG [1].

In Lin's review [2] on the low-profile vortex generator, it was mentioned that a device like MVG could alleviate the flow distortion in compact ducts to some extent and control boundary layer separation due to the adverse pressure gradients. Similar comments were made in the review by Ashill et. al. [3].

The formal and systematic studies about the micro VGs including micro ramp VG can be found in the paper of Anderson et al. [4]. Micro-actuators including MVG were found to have comparable effects as the boundary layer bleeding technique, and so MVG was considered to be very practical for the flow control in supersonic inlets. A series of experimental and computational investigations have been carried out since then. It is reported that Babinsky [1, 5, 6, 7] did the very prominent experimental studies. He made a series of experiments on different kinds of micro VGs and investigated their control effects in detail. The mechanism of MVG flow control from his work concludes that a pair of counter-rotating primary streamwise vortices is generated by MVG, which are mainly located within the boundary layer and travel downstream for a considerable distance. Secondary vortices are located underneath the primary ones and even more streamwise vortices could be generated under suitable conditions. Streamwise vortices inside the boundary later bring low momentum fluid up from the bottom and high momentum fluid down to the boundary layer.

A striking circular momentum deficit region is observed in the wake behind the MVG. The vortices keep lifting up slowly, which is thought to be the consequence of the upwash effect of the vortices.

Numerical simulations have been made on MVG for comparative study and further design purposes. Ghosh, Choi and Edwards [8] made detailed computations under the experimental conditions given by Babinsky. These numerical studies include RANS computations and hybrid RANS/LES computations using immersed boundary (IB) techniques. The fundamental structures, like the streamwise vortices and momentum deficit, were reproduced by the computation. Lee et al. [9] also made computations on the micro VGs problems by using Monotone Integrated Large Eddy Simulations (MILES). In their computation, the MVG is placed in a domain with the configuration following the real wind tunnel. The fundamental wave system of the MVG were reproduced in the computation, which consists of the main shock, expansion waves and re-compression shock like that reported by Babinsky [7]. The momentum deficit was captured too. They [10] further tested several variations of the standard MVG and micro vane to enhance the control effect.

Supersonic ramp flow is a typical prototype SBLI problem, and the ramp configuration often exists in the engine and control surfaces in high speed vehicles. The fundamental problem of the ramp flow includes the determination of characteristics and criteria of the flow separation and reattachment, the mechanism of the shock unsteadiness and the aerodynamic/thermal correspondence, etc. Many experimental studies had been made on these problems. Some well recognized ones can be found from the work by Dolling [11, 12, 13], Settles [14], Dussauge [15], Andreopoulos [16], Loginov [17] and their collaborators. For numerical simulations, there are three basic categories, i.e., the RANS, LES and DNS. It is well-known that RANS models do not perform well for SWTBLI (Wilcox [18] , 1993). According to Zheltovodov's opinion [19], the existing RANS models cannot solve the strong SBLI problem accurately, including the supersonic ramp flow. About the numerical works of LES, Rizzetta and Visbal [20].made simulations on a compression corner by implicit LES using a high-order method; Kaenal, Kleiser, Adams, and Loginov et al conducted LES [21, 22] on ramp flow using an approximate de-convolution model developed by Stolz. The comparisons were made and some agreement was obtained between the computational and the available experimental results. The first DNS on supersonic ramp flow was made by Adams for a 10°compression ramp at M=3 and Re_θ=1685. In the work done by Adams [23] and his colleagues, the 5_{th} order hybrid compact-ENO scheme was applied. Later Martin and the collaborators made a series of remarkable investigations by using DNS [24, 25, 26, 27, 28]. Comparisons were made between the computation and the experiments from the low Reynolds number wind tunnel at Princeton University [29]. They used the fifth order bandwidth-optimized WENO scheme which is the same scheme that the current work uses. The effect of low Reynolds number on the separation was studied. More work on MVG and other flow control tools have been done recently [30, 31, 32, 33, 34, 35]. According to the experimental and numerical research, some flow mechanisms are recognized as: a) the amplification of the turbulence after the SBLI is thought to be caused by the nonlinear interaction between the shock wave and the coupling of turbulence, vorticity and entropy waves [36]; b) the unsteady motion of the shock is considered to be generated by the very long low-momentum coherent structures in logarithmic layer and such structures might be formed by the hairpin vortex packet.

Although there are experiments and computations on MVG and ramp problems, these investigations were carried out separately. The combination of MVG and ramp is not conducted yet and it is unclear if the MVG can be used to control the supersonic ramp flow. In order to carry out flow control more effectively using MVG, the mechanism of the flow should be carefully studied first. There are at least three problems which should be clarified: a) what is the three-dimensional structures of the wave system caused by MVG. Till now, only two-dimensional structural information was available and confirmed by experiment; b) what is the relation between the momentum deficit and the flow structure and where does the low speed fluid come from? c) Is there any new mechanism besides the pronounced momentum transportation and mixing by streamwise vortices?

In this study, we try to understand the mechanism of the flow structure especially the vortex structure behind the MVG. Numerical simulations are made on supersonic ramp flow with MVG control at M=2.5 and Re_θ =5760. The trailing edge declining angle of the MVG is 70° in computation. In order to make simulations, a kind of large eddy simulation method is used by solving the unfiltered form of the Navier-Stokes equations (NSEs) with the 5th order bandwidth-optimized WENO scheme, which is generally referred to the so-called implicitly implemented LES. Without explicitly using the subgrid scale (SGS) model as the explicit LES, the implicitly implemented LES uses the intrinsic dissipation of the numerical method to dissipate the turbulent energy accumulated at the unresolved scales with high wave numbers. There are two main subfields about this category, i.e., the MILES [37, 38, 39, 40] by Boris, Fureby and Grinstein, et al, and the implicit LES [41, 42] by Visbal, Rizzetta and Gaitonde, et al. The first subfield is based on modified equation analysis, and typically uses the high order monotone scheme like flux-corrected transport (FCT) scheme or piecewise parabolic method (PPM). The ENO algorithm was also reported being used as the limiter in Ref.[40]. This kind of method can be used to solve the supersonic problems with shock waves, but the order of the scheme should not be competitive to the modern high order schemes like the compact schemes or WENO schemes with 5_{th} order of accuracy or higher. The second one [41] specifically uses the high order compact scheme by Lele and the high order Pade-type low-pass spatial filter. However, the published applications of the method are only for the low speed flow. When the same numerical algorithms were used on supersonic problems [43, 44], the Smagorinsky dynamic SGS model was incorporated in the simulation, which implies the existence of issues related to the numerical stability. A series of shock-capturing schemes were also tried for large eddy simulation [45, 46], including the WENO scheme. As mentioned in Ref. [46], at low Mach number the investigated compact differencing and filter scheme formulation may give better results but as the Mach number increases the relative suitability of the ENO method increases. However, the ENO scheme still produces numerical turbulence thus stabilizing filters is need, while the WENO scheme does not need filtering. Recently, an evaluating computation was reported on circular cylinder flow using implicitly implemented LES by the 5_{th} WENO scheme [47]. Comparisons were made between the computation and the experiment. The results show that the numerical algorithm is feasible and efficient. For the studied supersonic MVG controlled ramp flow problem, there are complex shock wave system, strong shock-vortex interaction and small scale structures. Considering the above status of implicitly implemented LES, the method by solving the NSEs with the 5_{th} order bandwidth-optimized WENO scheme is used in the paper and considered as certain implicitly implemented LES.

In our previous paper [48] , the flow field around the MVG and surrounding areas has been studied in details. Further more, 3-D structure of the shocks is also obtained by our numerical simulation [48].

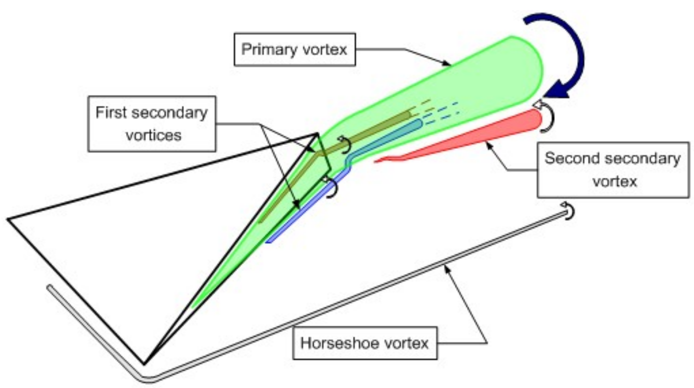

Figure 1: The dynamic vortex model (Li and Liu [2])

2 Numerical Simulation

2.1 Validation of the LES Results

The hairpin vortex was formed and then travelled downstream. According to the analyses, a dynamic vortex model can be given in Fig.1 (half domain). The dominant vortex near the MVG is the primary vortex; underneath there are two first secondary counter-rotating vortices, which later leave the body surface and become fully 3D separations by the way of spiral points in body surface. These vortices will merge into the primary vortex propagating downstream, while new secondary vortex will be generated under the primary vortex. This dynamic vortex model is mostly confirmed by the experiment work of Mohd R. Saad [49] et al. in recent (Fig. 2).

After the MVG, a strong momentum deficit was found behind MVG which causes a strong circular shear layer [1, 48], as shown in Fig. 3. The result is in consistency with the referenced computations and

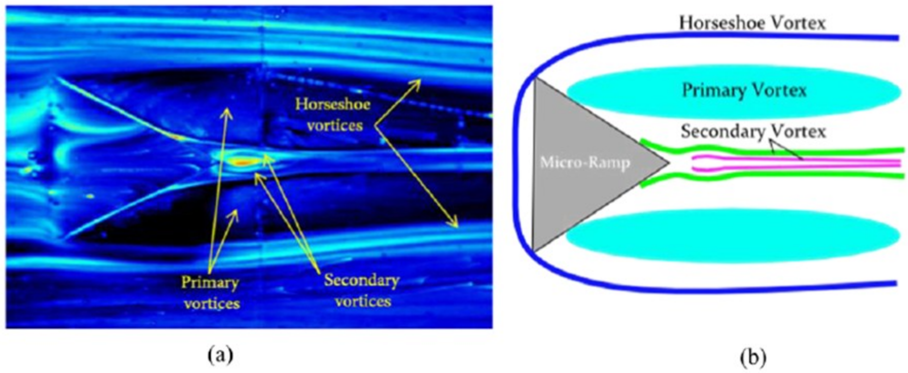

Figure 2: Surface flow visualization image and the vortex model given by Mohd R. Saad et al. [32]

experiments [8, 10, 48]. For clarity, the typical structure of the deficit is provided in Fig. 3 as well with spanwise streamlines. Inside the deficit area, there are two counter-rotating primary vortices which are illustrated in Fig. 3. In adjacent MVG region, the shape of deficit appears to be a circle, and usually has a root connected to the boundary layer. At underneath of the circle, there are two streamwise high velocity regions. Fig. 4 gives a qualitative comparison with experiment (Babinsky et al. [1], 2009) in the time and spanwise averaged velocity profile behind MVG. Qualitative agreement is achieved.

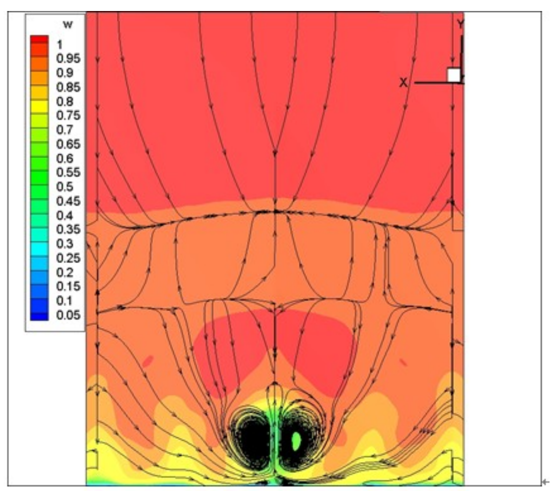

Figure 3: The momentum deficit

To reveal the coherent structure of the flow, the iso-surface of λ_2 scalar field is given in Fig. 5. It is very clear that there is a chain of vortex rings, starting from behind of the trailing-edge of MVG. The rings are generated almost erectly at first and then they will be continuously distorted and enlarged while propagating downstream. These rings could be a dominant factor of the mechanisms of MVG in control of shock boundary layer interaction.

Fig. 6 demonstrates the instantaneous numerical schlieren at the central plane. We can see many vortex rings appear in circular shapes. Informed with the prediction of vortex rings, the experimentalists in UT Arlington used some technology to validate the discovery. They used the particle image velocimetry (PIV) and the acetone vapor screen visualization to track the movement of the flow. More specifically, the flash of a laser sheet is used to provide the light exposure at a time interval of micro seconds. Fig. 7 presents a typical image at the center plane using PIV and the acetone vapor technology (Lu et al. [52]). It is clearly demonstrated that a chain of vortex rings exists in the flow field after the MVG, same as shown in LES results (see Fig. 6).

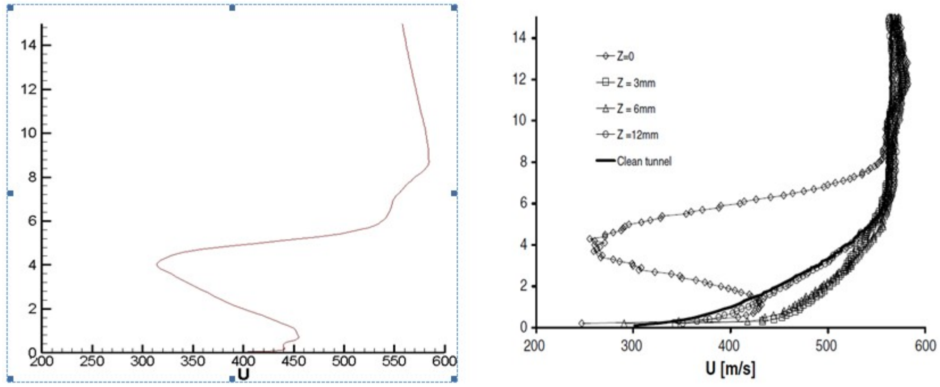

a) Averaged velocity profile behind MVG   b) Averaged velocity profile by Babinsky et al

Figure 4: Qualitative comparison of averaged velocity profile behind MVG with experiment

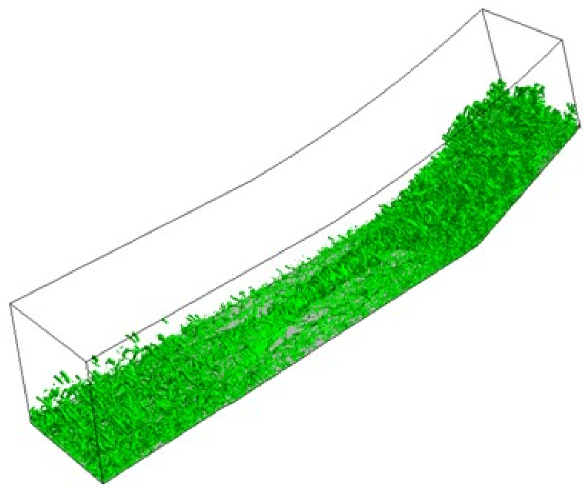

(a) Global view

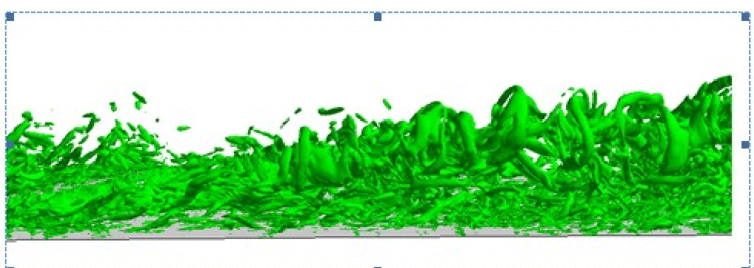

(b) Close-up view behind the MVG

Figure 5: Vortex rings shown by iso-surface ofλ_2

Our numerical discoveries of the vortex ring structures are also confirmed by 3-D PIV experiment (Fig. 8) conducted by Sun et al at Delft University [53]. Compared the two results, we can find the similar distribution of streamwise (ω_z) and spanwise vorticity (ω_x) components, which also proves the existence of ring structures. The Kevin-Helmholtz vortices part in Fig. 9 corresponds with the ring head in Fig. 5. The underneath part which is illustrated as streamwise vortices are two counter rotating primary vortices which are considered to be the main source of the ring structure as explained later .

However the vorticity component which revolves towards the vertical direction (ω_y in our case) is not

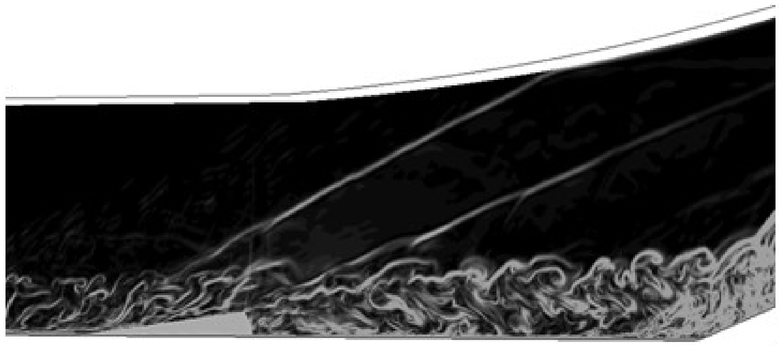

Figure 6: The numerical shilieren at the center plane

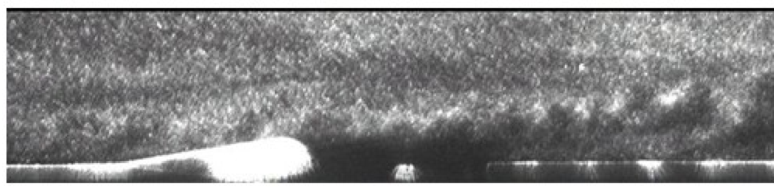

a) Using PIV

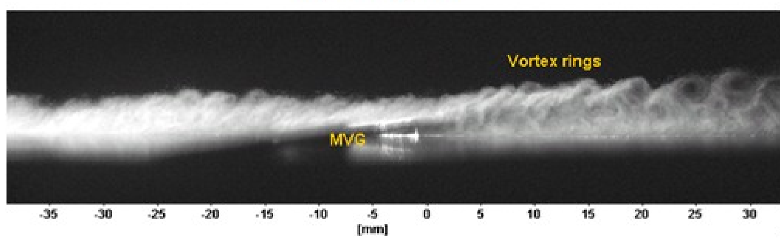

b) Using the acetone vapor

Figure 7: The laser-sheet flash image at the center plane (Lu et al 2010)

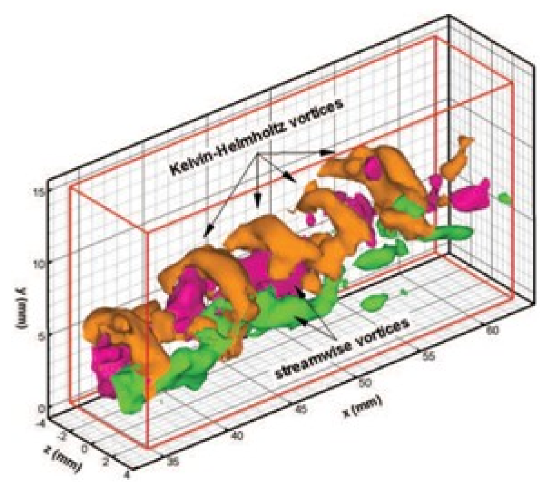

Figure 8: K-H rings behind MVG by (Sun et al 2011)

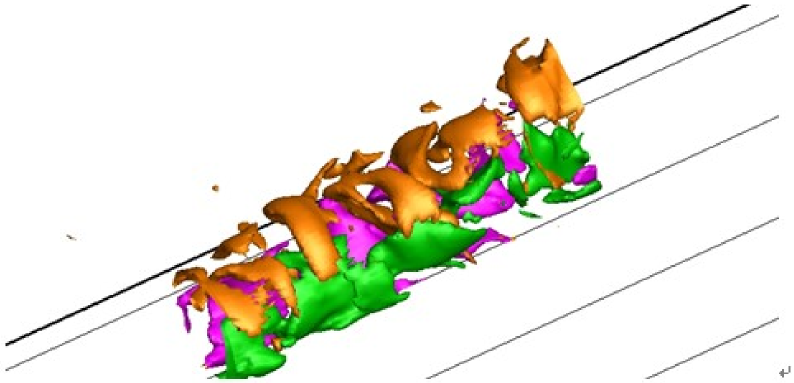

Figure 9: Distribution of Kelvin-Helmholtz vortices and streamwise vortices from LES

shown in Fig. 9. If this missing part was provided, we can see the vortex ring structure clearly by the combination of all the components of vorticity as shown in Fig. 10 which is in accordance with the structure in Fig. 5.

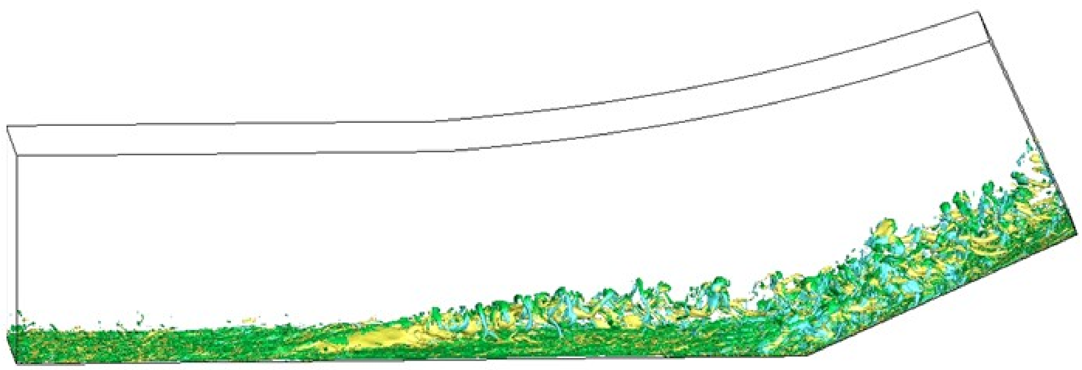

a)global view

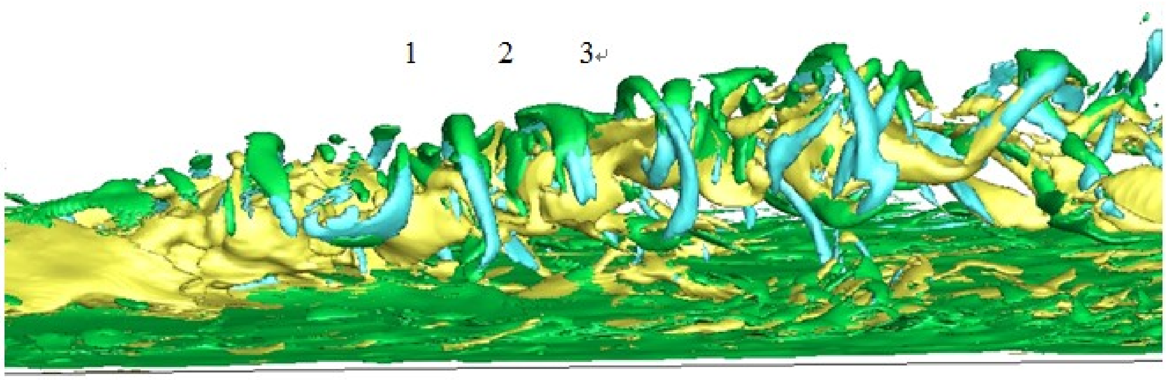

b) close-up view

Figure 10: Vortex rings shown by the components of vorticity

The newly generated vortex ring discussed above will immediately interact with the shock wave induced by the ramp. Vortex-shock wave interaction [54] has been studied for a while. Main concerned issues in this topic are: a) the deformation of the shock wave; b) the multistage features of the interaction caused by the vortex interaction with the primary shock and the reflection shocks, etc; c) the acoustic characteristics, which includes near- and far-field of acoustic, the dipole and quadruple acoustic pressure structure, etc.

Compared with the classic study Ref. [55, 56, 57], the vortex rings-shock interaction of the MVG controlled ramp flow is a different case and could bring a new topic for research. The differences are: a) the interaction is a more complicated 3-D case than the 2-D counterpart, which happens between 3-D vortex rings and the oblique shock waves; b) the interaction happens within or close to the boundary layer and the separation region, where other flow structures exist like vortices with small scale of turbulence besides the shock wave; c) the interaction is a continuous process, not a one-time event; d) besides the rings, components of the primary vortices still exist and make the interaction more complicated. Although differences are obvious, results obtained in the standard vortex ring-shock interaction can still give hints and suggestions to the current research.

It is definitely necessary to find physical mechanisms of MVG for design engineers. RANS, DES, RANS/DES, RANS/LES, etc are good engineering tools, but they may not be able to reveal the mechanism and get deep understanding of MVG. We need high order DNS/LES. A powerful tool is the integration of high order LES and experiments. In this paper, an approach called monotone integrated LES (MILES) [9, 40] was adopted at Mach number 2.5 and Re_θ =5760, in which the numerical dissipation is used as the sub-grid stress model.

Flows around MVGs are studied with back edge declining angle 70° (see Fig. 11). The geometries for the cases are shown in Fig 12. (in which δ_0 represents the incompressible boundary layer nominal thickness). A general grid partition technique is used in this grid generation. According to experiments by Babinsky[1], the ratio h/δ_0 of the models range from 0.3 to 1. The appropriate distance from the trailing-edge to the control area is around 19 56h or 8 19 δ_0. In this study, the height of MVG h is assumed to be $\delta_0/2$ and the horizontal distance from the apex of MVG to the ramp corner is set to be $19.5h$ or $9.75\delta_0$. The distance from the end of the ramp to the apex is 32.2896h. The distance from the starting point of the domain to the apex of MVG is $17.7775h$. The height of the domain is from 10h to 15h and the width of the half domain is 3.75h. As shown in Fig. 6, three regions are divided as: the ramp region, MVG region and fore-region. Between each two regions, there is a grid transition buffer. Because of the symmetry of the grid distribution, only half of the grids need to be generated. The grid number for the whole system is: $n_{spanwise} \times n_{normal} \times n_{streamwise} = 128 \times 192 \times 1600$. Using the inflow flow profile described in the next section, a data summary is given in table 1 about the geometric parameters of the grid system.

2.2 Numerical methods, Grid and Turbulent inlet

The details about the geometric objects, grid generation, computational domain, etc, which are introduced in our previous paper, [48, 49] will not be repeated here.

The adiabatic, zero-gradient of pressure and non-slipping conditions are adopted at the wall. To avoid possible wave reflection, the non-reflecting boundary conditions are used on the upper boundary. The boundary conditions at the front and back boundary surfaces in the spanwise direction are treated as the periodic condition, which is under the consideration that the problem is about the flow around MVG arrays and only one MVG is simulated. The outflow boundary conditions are specified as a kind of characteristic-based condition, which can handle the outgoing flow without reflection [50, 51].

Table 1: The geometric parameters for the computation

L_x	L_y	L_z	Δx	Δy	Δz
$3.75\delta_0$	$5-7.5\delta_0$	$25.03355\delta_0$	26.224	$1.357-38.376$	12.788

New fully developed turbulent inflow boundary conditions are generated in this paper using following steps:

- a) A turbulent mean profile is obtained from previous DNS simulation results [8] for the streamwise velocity (w-velocity) and the distribution is scaled using the local displacement thickness and free stream velocity. The basic transfer is based on the assumption that the same distribution exists between the relations of U/U_ε y/θ^* . And the averaged streamwise velocity of MVG case can be reached by interpolation (3rd Spline interpolation);

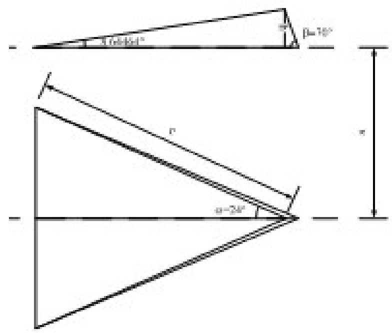

Figure 11: The sketch of MVG at $\beta = 70°$

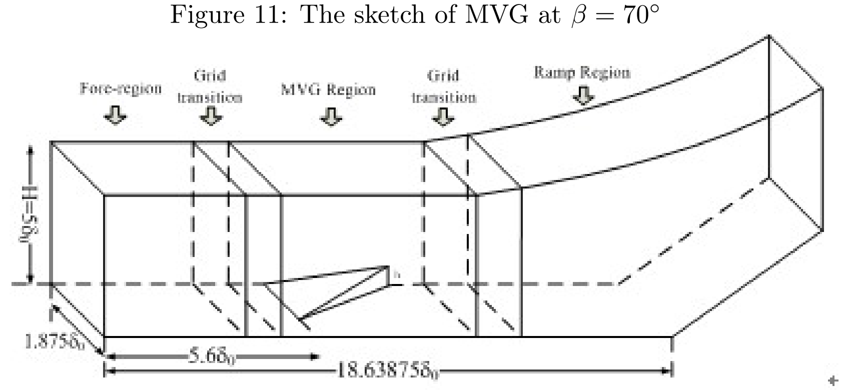

Figure 12: The schematic of the half grid system

- b) The pressure is uniform at inlet and has the same value as the free stream value. The temperature profile is obtained using WalzâĂŹs equation for the adiabatic wall: first, the adiabatic wall temperature is determined using: $T_w = T_\varepsilon(1 + r(\gamma - 1)/2 \times M_\varepsilon^2)$, where the subscript ε means the edge of the boundary layer and r is the recovery factor with value 0.9; next, the temperature profile is obtained by Walz's equation: $T/T_\varepsilon = T_w/T_\varepsilon - r(\gamma - 1)/2 \times M_\varepsilon^2(U/U_\varepsilon)^2$;
- c) The fluctuation components of the velocity are separated from the total velocity at every instantaneous data file (totally 20,000 files). And such fluctuations are rescaled in the same way. Because $\overline{T}/T_\varepsilon - r(\gamma-1)/2 \times M_\varepsilon^2(\overline{U}/U_\varepsilon)^2$, considering the non-dimensional form and ignore the T_ε and U_ε , we get $d\overline{T} = -r(\gamma - 1) \times M_\varepsilon^2 U d\overline{U}$, or $\Delta T = -r(\gamma - 1) \times M_\varepsilon^2 \Delta U$ .Density fluctuation is determined by $\frac{\Delta\rho}{\overline{\rho}} = -\frac{\Delta T}{\overline{T}}$;
- d) Finally, the transformed parameters are $u = U + \Delta u$,$v = V + \Delta v$,$w = \Delta w$,$rho = \overline{\rho} + \Delta\rho$, $p = \frac{\rho T}{\gamma M^2}$, $T = \overline{T} + \Delta T$.

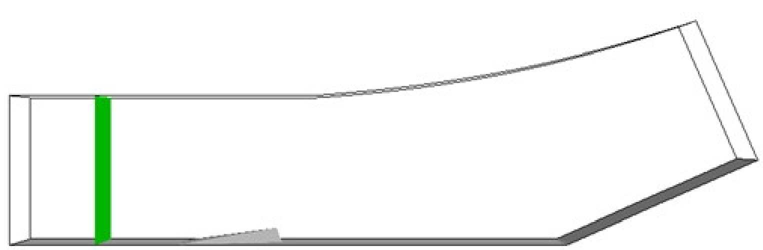

Figure 13: The spanwise cross section on which the flow parameters are checked

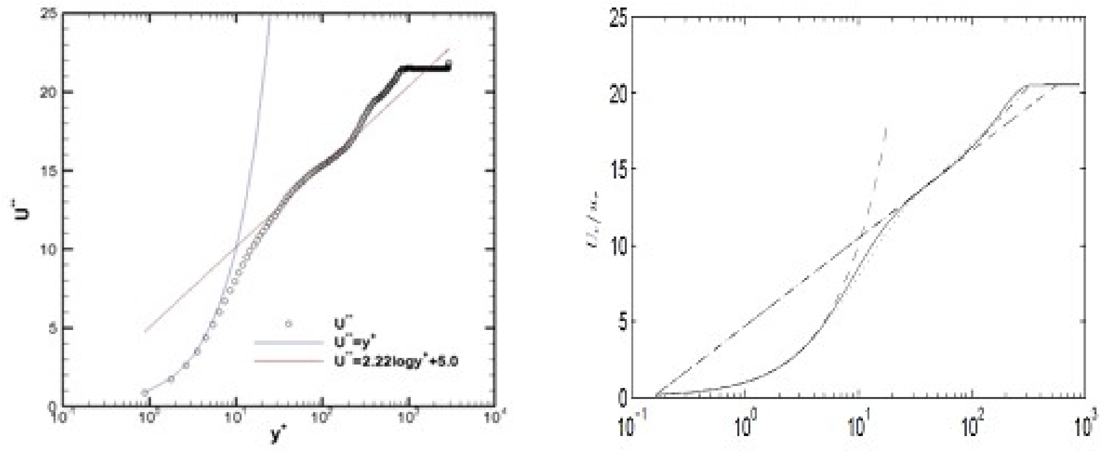

Figure 14: Inflow boundary-layer profile comparison with Guarini et al's

To check the flow properties before the MVG, we analyzed the relevant flow parameters on a spanwise cross section which is illustrated in Fig 13. The cross section is $11.97h$ ahead the apex of MVG. As a result, the displacement thickness $\delta^* = 0.371h$, the momentum thickness $\theta = 0.275h$, nominal boundary layer thickness $\delta = 2.36h$. Thus, we can obtain a shape factor H as about 1.35, which shows the flow before the MVG is fully developed turbulence flow.

Fig. 14 shows the inflow boundary layer velocity profile in log-coordinates on the same cross section. There is a well-defined log region and the agreement with the analytical profile is well established. These results are typical for a naturally grown turbulent boundary layer in equilibrium [58]. Fig. 15 gives the vortex structure of the inlet flow shown by the iso-surface of λ_2.

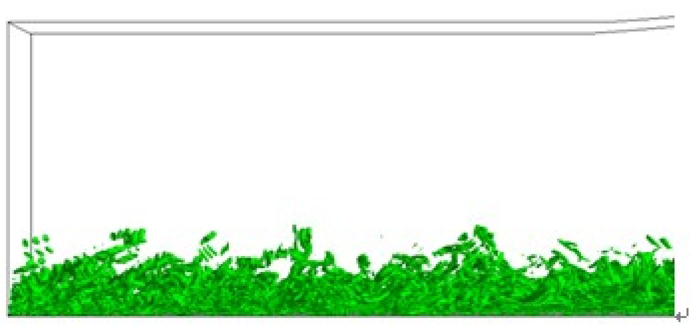

Figure 15: The vortex structure of the inlet flow shown by the iso-surface of λ_2

2.3 Influence on the ring structure by the interaction

In order to make further analyses, it is necessary to get the kinetic information of the vortex rings. According to the results of computation, it is found that vortex rings appear irregularly after the MVG and before the ramp. They are continuously distorted during propagating. Thus, only 3 of these rings (marked in Fig. 13b) are checked since they are relatively regular at this stage. It shows that they almost propagate in the same speed and the averaged parameters are presented in table 1.

The shape of vortex rings is badly deformed before they penetrate the shock wave and travel along the ramp. The speed of the two vortex rings before and after the shock can be found approximately (see Fig. 16, marked as 1 and 2), and the value of the streamwise velocity is: $V_{ring1} \approx 0.77U_\infty, V_{ring2} \approx 0.47U_\infty$.

For the second ring, $V_{ring,2}$ is the streamwise velocity component, and the velocity along the ramp

Table 2: Characteristic parameters of vortex rings on the plate

Δs_{ring}	$V_{ring,1}$	$T_{ring}(h/U_\infty)$	St_h
$1.21h$	$0.78U_\infty$	1.55	0.26

direction is really about $0.68U_\infty$. The value is in consistency with the common knowledge, i.e., typical convective structures usually travel at a speed around $0.7U_\infty$. For the first velocity $V_{ring,1}$, the result has the same quantity level as the common sense. We can also find that the total speed of the ring dose not change much when it penetrates the shock wave. The little decrease to the velocity may be caused by the interaction between ring and viscous sub-layer since the rings intrude into the lower layer in the boundary layer after they penetrate the shock. This is partially because the shock is significantly weakened and almost disappeared when the rings come.

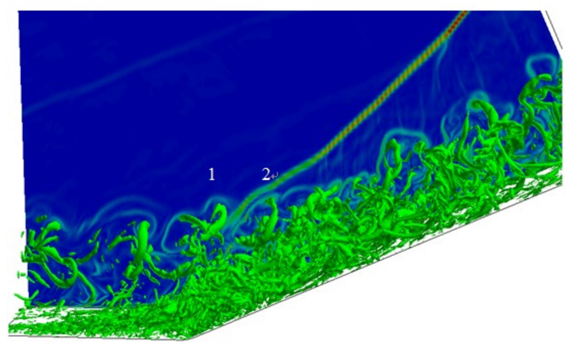

Figure 16: Two vortex rings above the ramp for measurement

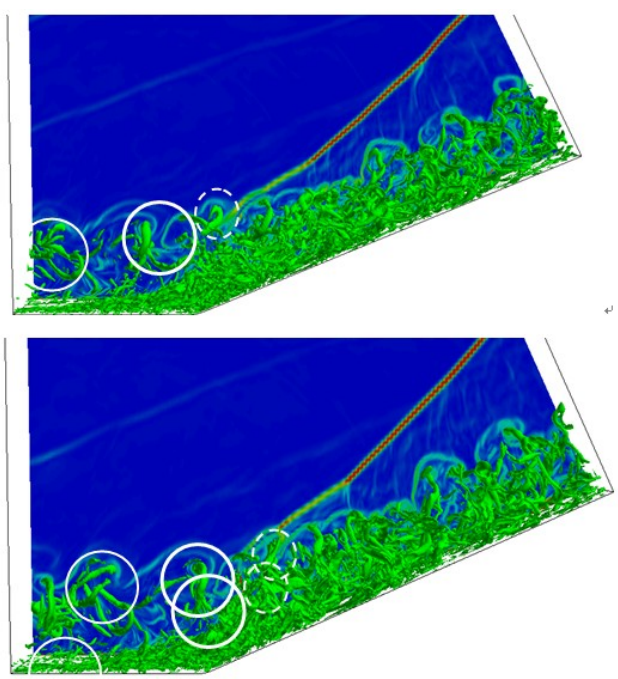

Figure 17: The 3D view of the propagating rings at the ramp part at different time

In Fig. 17, we tracked 3 different rings when they are moving. When the vortex ring is passing through the shock wave, the vortex structure is slightly distorted. The vortex ring does not break down by penetrating the strong shock wave and even keeps its original topology very well. Since the vortex ring is distorted continuously after it is created and propagating downstream (as we can find in Fig. 17, the first ring in circle), there's no evidence that the interaction of vortex rings and shock is the reason to cause the ring distortion. The distortion of rings could be caused by the boundary layer flow or the compressing effect of the ramp. In Fig. 17 and Fig. 18, we can also find that those vortex rings exist after penetrating the shock wave and their topology are well maintained as far as the end of the ramp. That means that, for 3-D shock boundary interaction, shock rarely affects the vortex structure. Fig. 19 shows the streamwise vorticity distribution at the central plane right before and after a vortex ring penetrates the shock wave, from which we can find that the shock rarely determines the evolution of the vortex rings. At the head part and the vorticity distribution is not changed much. Those rings pass the shock wave rather smoothly. This is because the shock only generates great gradients of v, t and p in the normal direction, but not new shear layer or vorticity.

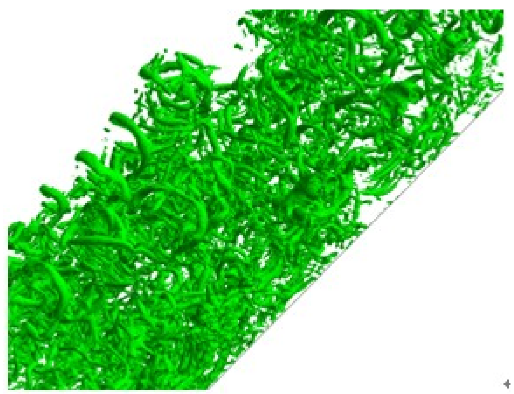

Figure 18: The ring structure at the ramp part by λ_2

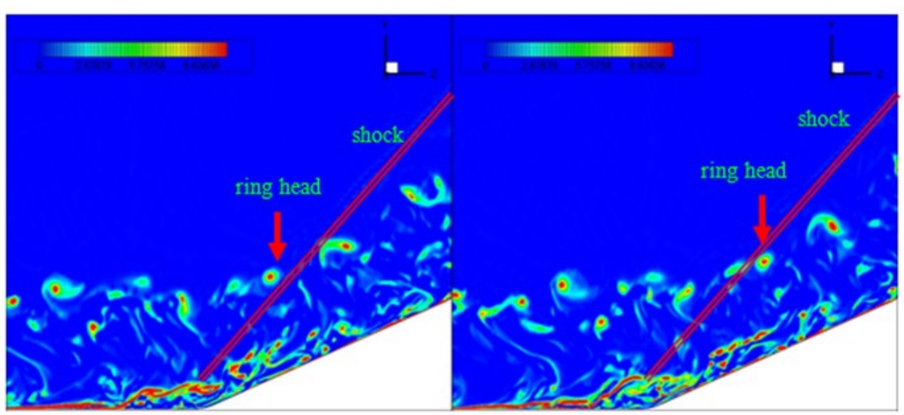

Figure 19: Streamwise vorticity distribution at two different time steps

The interaction between the vortex rings and shock waves can be explained with Richtmyer-Meshkov instability (RMI) to some extent. It occurs when an interface between fluids of differing density is impulsively accelerated, e.g. by the passage of a shock wave. The vortex rings structure is a wave of differing densities. The process of passing the shock wave is the same with that in RMI theory. The key point of RMI is the baroclinic effects between $\nabla\rho$ and ∇p .

$$\frac{d\Omega}{dt} - (\Omega\cdot\nabla)\mathbf{v} + \mathbf{\Omega}(\nabla\cdot\mathbf{v}) = \nabla\times\mathbf{F} + \frac{\mathbf{1}}{\rho^{\mathbf{2}}}\nabla\rho\times\nabla\mathbf{p} + \nabla\times\ (\nu\nabla\mathbf{v}) + \frac{\mathbf{1}}{\mathbf{3}}\nabla\times(\nu\nabla\times(\nabla\cdot\mathbf{v}) \tag{1}$$

The quantity of $|\nabla\rho\times\ nablap|$ plays a very important role to the vorticity disturbance. Actually, it is the most important source term in the process of vorticity variation (Eq. 1) in our case. Fig. 20 shows the iso-surface of $|\nabla\rho\times\ nablap|$ with different values. From that figure, we can find that: a) the large value of $|\nabla\rho\times\ nablap|$ only exists in a small area, and thus the flow field, especially the vortex structure, is rarely affected. b) The small value of $|\nabla\rho\times\ nablap|$ mainly happens in the bottom of the boundary layer so that the shock wave will not change the vortex rings much while those rings only exist on the upper side of the boundary layer. The ring structure is robust and never breaks down even when it penetrates the strong shock wave.

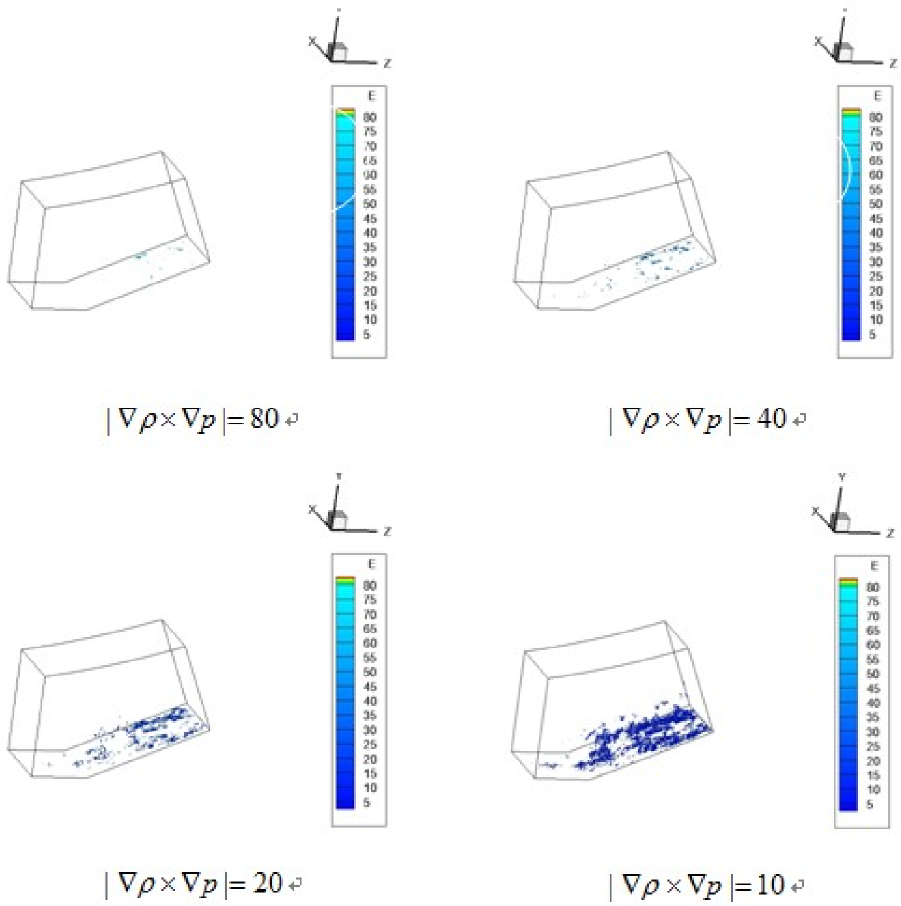

Figure 20: Iso-surface of in the ramp part

From all discussed above, we can conclude that the vortex ring and shock interaction, even with strong shock wave, does not influence the ring structure much. Those rings keep their shapes, the quantity of vorticity, and also travel normally pretty much like that the shock is absent. However, after penetrating the shock wave, the quantity of density and pressure gradient seems increased in the ring structure as seen in Fig. 21.

2.4 Influence on oblique shock wave

As newly found structure, the string of vortex rings are fully 3D structures. Thus the interaction with shock wave has different features from classic 2-D ones.

To better illustrate the process, two kinds of sections are investigated: the centre plane (Fig. 22) and then a series of spanwise computational planes (Fig. 23) with constant streamwise index. In Fig. 22, the gradient fields of density $|\nabla\rho|$ and pressure $|\nabla p|$ at two different moments are depicted to analyze the

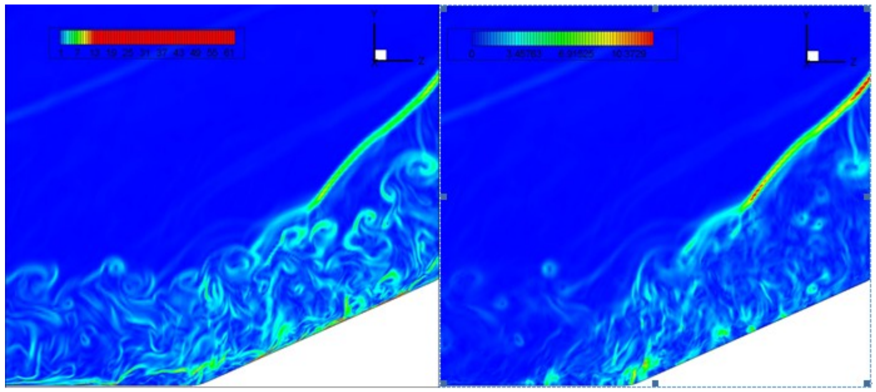

Figure 21: Density gradient (left) and pressure gradient (right) on the central plane

interaction. Fig. 23 gives the contour of and of three spanwise computational planes. In order to get the overall understanding of the interaction, it is also necessary to directly give the 3-D shape of the shock wave. In Fig. 24, six snapshots are obtained using the iso-value of pressure. The value of pressure is selected to make the inner shock layer be seen from outside. The shape of the strong shock wave is given by $|\nabla p|$ in Fig 25.

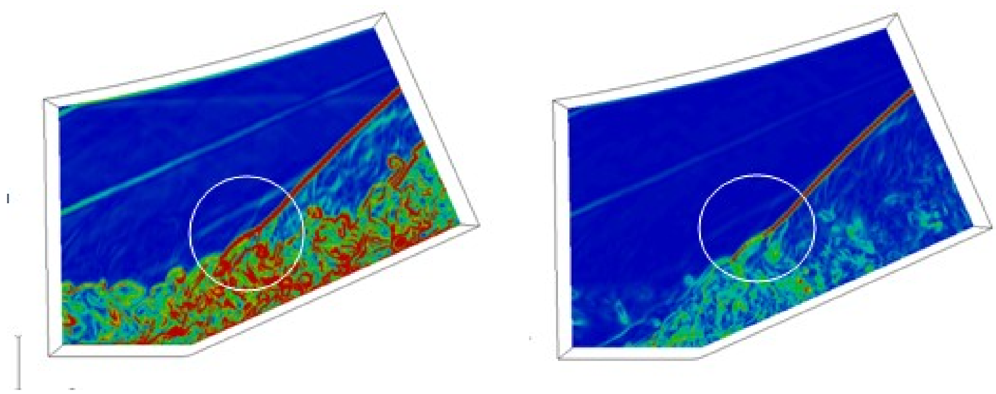

t_1 t_1

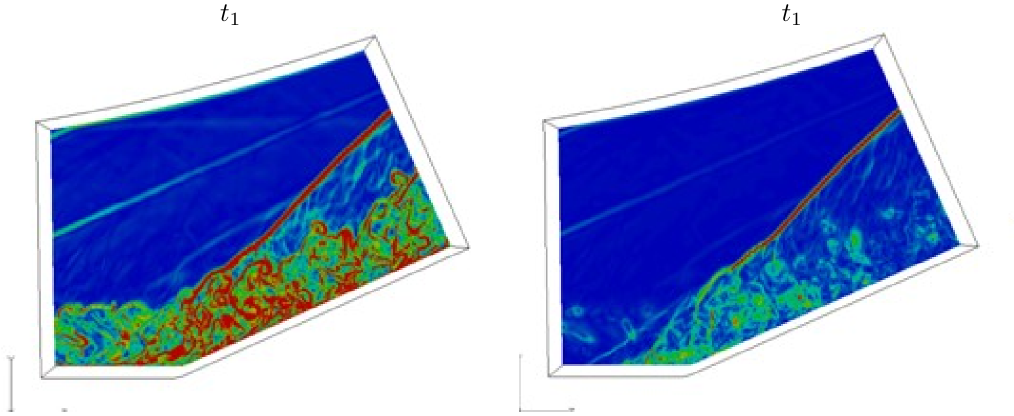

t_2 t_2

$a)|\nabla \rho|$ $b)|\nabla p|$

Figure 22: Contours of $|\nabla \rho|$ and $|\nabla p|$ at two moments at the center planes

From the figures, the following features can be observed:

1) In Fig. 22, it demonstrates that there are at two layers of shock wave or wave structures after the

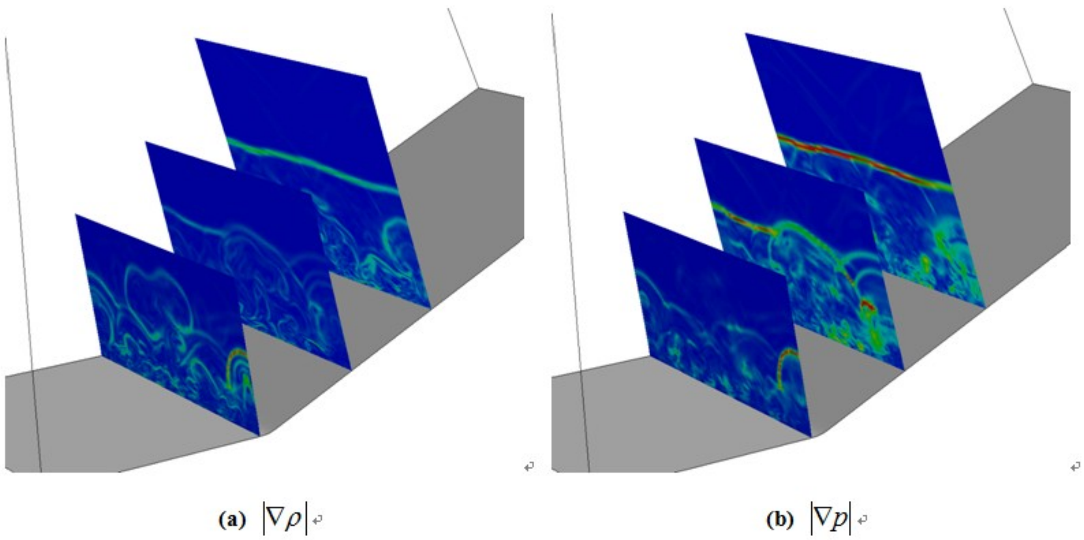

Figure 23: The contours of $|\nabla\rho|$ and $|\nabla p|$ at spanwise sections and at four successive moments

ramp corner: upper one is the original but quite weaker separation/reflection shock; the lower other is the stronger interacting shock wave caused by the vortex rings. These two layers of shocks will merge into one shock wave afterwards, which is the oblique shock caused by ramp.

2) Comparing Fig. 22(a) and (b), especially in the front section, it can be found that there is a slip line under the curved shock in the contour of $|\nabla\rho|$, which cannot be found in the contour of $|\nabla p|$. The slip line indicates the density change across the line, while the pressure keeps the same at the both sides of the line. After checking the movie about $|\nabla\rho|$, we found the slip line comes from the original connections between vortex rings.

3) In Fig. 23, we can found that when a vortex ring penetrates into the shock wave, the interaction part of the shock is distorted and its intensity is also significantly reduced.

4) In Fig. 24 and Fig. 25, it shows that the interaction between shock wave and vortex rings is in fully 3D. The flow field lost its symmetry, which can be clearly illustrated by the shape of shock wave. 3-D shape of the multilayer structures and bumps is one of the typical characteristics of the shock-vortex interaction.

5) In Fig. 25 it can be observed that, at the corner of the ramp, there is no obvious sign of shock waves and the original shock wave retreats to a downstream position on the ramp. This result shows that the separation/reflection shock wave is eliminated near the corner. We can see that it is induced by the interaction of the vortex rings and the viscous sub-layers (Fig. 24). This kind of phenomenon is a complicated turbulence-shock wave interaction.

6) When the vortex rings pass through the shock wave (Fig. 24 at time t1), the shock wave will be distorted like a bump (Fig. 24 at time t_3), and the bump will be gradually smoothed when propagating downstream. We can clearly see that this shape is caused by the vortex ring and shock wave interaction. When the vortex enters the shock wave and moves away from it, the distortion subsides quickly. The subsequent incoming vortices will repeat the process. At the fifth section in Fig. 24, the bump shape is less observable, which indicates the vortex group moves in a position far below the shock wave and have less influence on the separation/reflection shock wave.

To explain the mechanism of the bump shape of the 3D shock wave, in Fig. 25, the second ring in Fig. 16 (marked as 2) is taken out and the flow filed on a spanwise cross section, which pass through the center of this ring, is plotted in Fig 26. The velocity field is the tangent projection of the 3D velocity vector distribution on the cross section which ignores the streamwise velocity component along the ramp direction. The projection of free stream velocity moves towards the ramp since the cross section is vertical to the ramp surface. Meanwhile, as noticed in Fig. 16, when the vortex rings enter the shock wave, they incline to some degree to the ramp. It is very interesting that the vector field shown in the section clearly demonstrates the upward induction of the flow at the center position of the ring. The inducted flow will interact with the

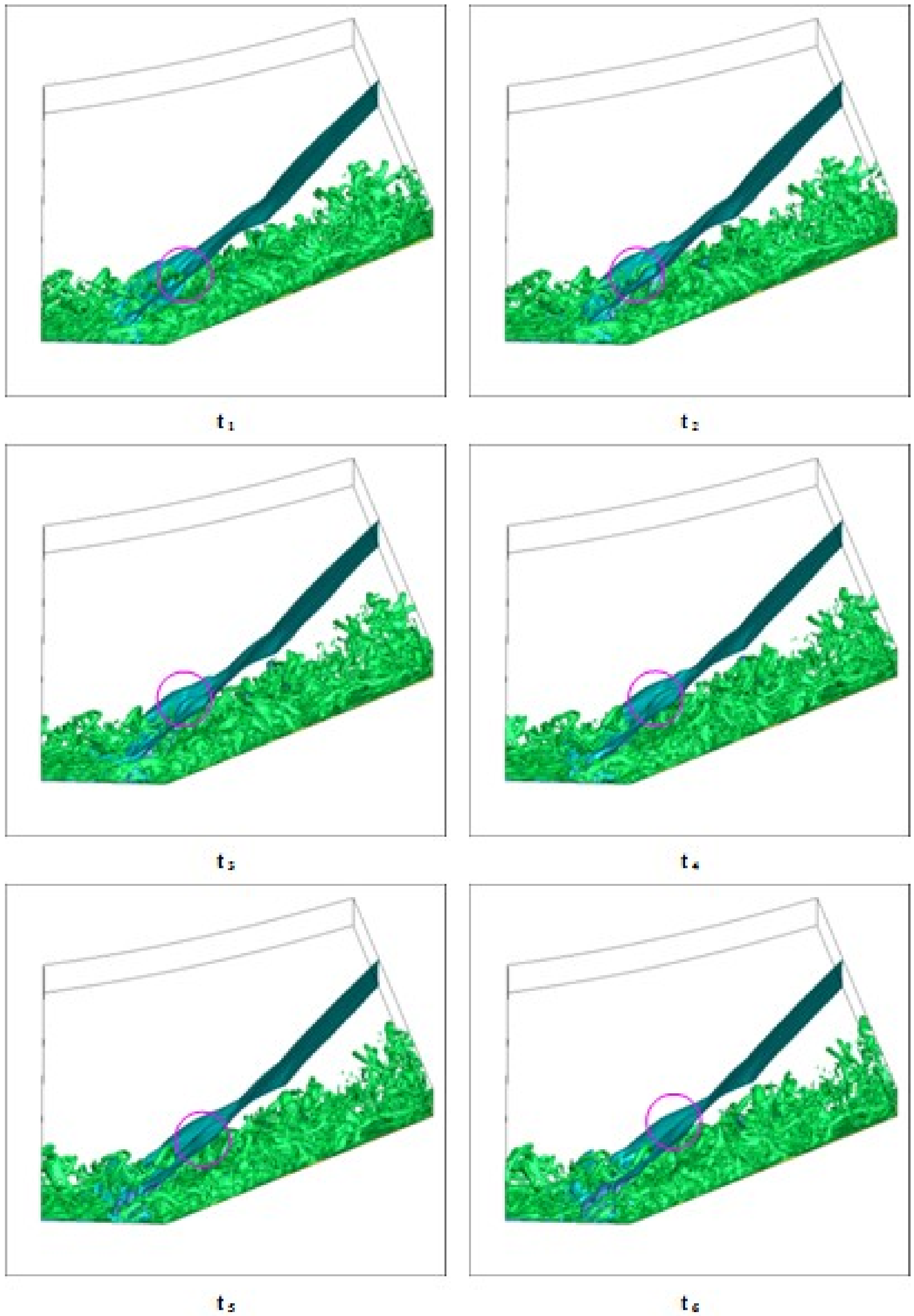

Figure 24: The shock wave shape by the iso-surface of pressure and ring structure by λ_2

incoming free stream and make the surface of the interaction which is the location of the shock wave to be an obvious arc-like shape. The existence of strong upwash component of flow field induced by the vortex ring will cause a bump-like shock wave Fig. 25 & Fig. 26).

3 Conclusion

The interaction between vortex ring structure and the oblique shock by the MVG controlled ramp flow at M=2.5 and Re=5760 is studied in this paper. It shows that the ring structure generated by MVG is very

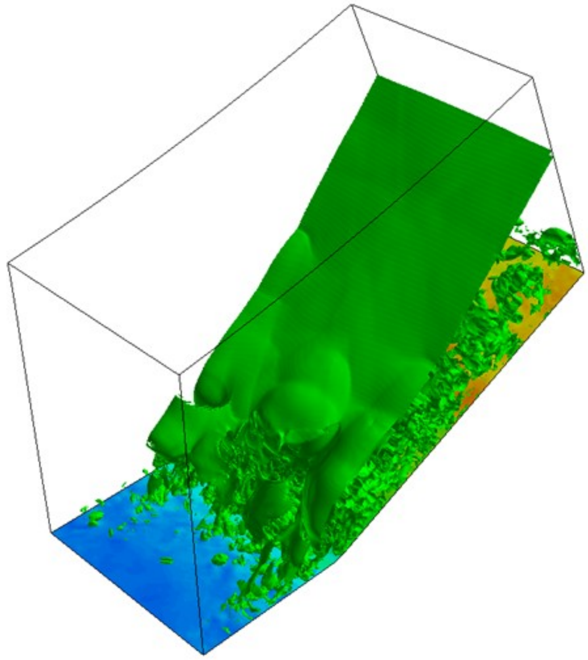

Figure 25: The 3D shock wave shape by $|\nabla p|$

stable, does not break down and keeps it original topology after penetrating the strong shock wave. However, the oblique shocks are broken when they interact with the vortex rings. The bump on the 3D shock wave surface is observed and its mechanism is explained as a result of the ring-like vortex induced flow field which has a strong upwash component. The separation zone, which is originally generated by the shock-boundary layer interaction, is significantly reduced due to the ring-shock interaction.

4 Ackonwledgements

This work was supported by The Department of Mathematics at University of Texas at Arlington. The authors are grateful to Texas Advanced Computing Center (TACC) for providing computation hours. This work is accomplished by using Code LESUTA which was provided by Dr. Chaoqun Liu at University of Texas.

References

[1] H. Babinsky and Y. Li and C. W. P. Ford. *Microramp Control of Supersonic Oblique Shock-Wave/Boundary-Layer Interactions.* AIAA J., 47(3):668-675, 2009.

[2] J. C. Lin. *Review of Research on Low-Profile Vortex Generators to Control Boundary-Layer Separation.* Progress in Aerospace Sciences, 38:389-420, 2002.

[3] P. R. Ashill and J. L. Fulker. *Hackett, K. C. :A Review of Recent Developments in Flow Control.* The Aeronautical Journal, 109:205-232, 2005.

[4] B. H. Anderson and J. Tinapple and L. Surber. *Optimal Control of Shock Wave Turbulent Boundary Layer Interaction Using Micro-Array Actuation.* AIAA Paper 2006–3197, 2010.

[5] H. A. Holden and H. Babinsky. *Vortex Generators Near Shock/Boundary Layer Interactions.* AIAA Paper 2004-1242, 2004.

[6] C. W. Ford and H. Babinsky. *Micro-Ramp Control for Oblique Shock Wave/Boundary Layer Interaction.* AIAA Paper 2007-4115, 2007.

[7] H. Holden and H. Babinsky. *Effect of Microvortex Generators on Separated Normal Shock/Boundary Layer Interactions.* AIAA J., 38: 389-420, 2002.
[8] S. Ghosh and J. Choi and J. R. Edwards. *RANS and Hybrid LES/RANS Simulations of the Effects of Micro Vortex Generators Using Immersed Boundary Methods.* AIAA Paper 2008-3726, 2008.
[9] S. Lee and E. Loth and C. Wang. *LES of Supersonic Turbulent Boundary Layers with ν VG's.* AIAA Paper 2007-3916, 2007.
[10] S. Lee and E. Loth. *Supersonic Boundary Layer Interactions with Various Micro-Vortex Generator Geometries.* AIAA Paper 2009-3712, 2009.
[11] D. S. Dolling and M. T. Murthy. *Unsteadiness of the Separation Shock Wave Structure in a Supersonic Compression Ramp Flow field.* AIAA J., 12:1628-1634, 1983.
[12] D. S. Dolling. *High-Speed Turbulent Separated Flows: Consistency of Mathematic Models and Flow Physics.* AIAA J., 36:725-732, 1998.
[13] D. S. Dolling. *Fifty Years of Shock-Wave/Boundary-Layer Interaction Research: What next?.* AIAA J., 39:1517-1531,2001.
[14] G. S. Settles and L. J. Dodson. *Supersonic and Hypersonic Shock/Boundary Layer Interaction Database.* AIAA J., 32:1377-1383, 1994.
[15] J. P. Dussauge and P. Dupont and J. F. Debieve. *Unsteadiness in Shock Wave Boundary Layer Interaction with Separation.* Aerospace Science and Technology, 10(2):85-91, 2006.
[16] J. Andreopoulos and J. H. Agui and G. Briassulis. *Shock Wave-Turbulence Interactions.* Annu. Rev. Fluid Mech., 32:309-345, 2000.
[17] M. S. Loginov and N. A. Adams and A. A. Zheltovodov. *Large-Eddy Eimulation of Shock-Wave/Turbulent-Boundary-Layer Interaction.* J. Fluid Mech, 565:135-169, 2006.
[18] D. Wilcox. *Turbulence Modeling for CFD.* DCW Industries, Inc., 1993.
[19] A. A. Zheltovodov. *Advances and Problems in Modeling of Shock Wave Turbulent Boundary Layer Interactions.* Proceedings of the international Conference on the Methods of Aerophysical research, Institute of Theoretical and Applied Mechanics, Novosibirsk, Russia, 2004.
[20] D. Rizzetta and M. Visbal. *Large Eddy Simulation of Supersonic Compression-Ramp Flow by High-Order Method.* AIAA J., 39(12):2283-2292, 2001.
[21] R.V. Kaenel and L. Kleiser and N. A. Adams and J. B. Vos. *Large-Eddy Simulation of Shock-Turbulence Interaction.* AIAA J., 42(12)2516-2528, 2004.
[22] M. Wu and M. P. Martín, *Direct Numerical Simulation of Supersonic Turbulent Boundary Layer over a Compression Ramp.* AIAA J., 45(4):879-889, 2007.
[23] N. A. Adams. *Direct simulation of the turbulent boundary layer along a compression ramp at $M = 3$ and $Re\ \theta = 1685$.* J. Fluid Mech, 420: 47-83, 2000.
[24] M. P. Martín. *Direct Numerical Simulation of Hypersonic Turbulent Boundary Layers. Part 1. Initialization and Comparison with Experiments.* J. Fluid Mech, 570:347-364, 2007.
[25] M. Ringuette and M. Wu and M. P. Martin. *Low Reynolds Number Effects in a Mach 3 Shock/Turbulent-Boundary-Layer Interaction.* AIAA J., 46(7):1884-1887, 2008.
[26] M. Wu and M. P. Martín. *Analysis of Shock Motion in Shockwave and Turbulent Boundary Layer Interaction Using Direct Numerical Simulation Data.* J. Fluid Mech, 594:71-83, 2008.
[27] M. J. Ringuette and M. Wu and M. P. Martín. *Coherent Structures in Direct Numerical Simulation of Turbulent Boundary Layers at Mach 3.* J. Fluid Mech., 47(5):59-69, 2008.
[28] S. Priebe and M. Wu and M. P. Martín. *Direct Numerical Simulation of a Reflected-Shock-Wave/Turbulent-Boundary-Layer Interaction.* AIAA J., 47(5):1173-1185, 2009.
[29] P. Bookey and C. Wyckham and A. Smits. *Experimental Investigations of Mach 3 Shock-Wave Turbulent Boundary Layer Interactions.* AIAA Paper 2005-4899, 2005.
[30] L.N. Cattafesta III and M. Sheplak. *Actuators for active flow control.* Annual Review of Fluid Mechanics, 43:247-272, 2011.
[31] P.L. Blinde and R. A. Humble and B.W. van Oudheusden and F. Scarano. *Effects of micro-ramps on a shock wave/turbulent boundary layer interaction.* Shock Waves, 19(6):507-520, 2009.
[32] R. Saad and E. Erdem and L. Yang and K. Kontis. *Experimental studies on micro ramps at Mach 5.* Paper 2816, Proceedings of the 28th International, Symposium on Shock Waves, Manchester, U.K., 17-32, 2011.
[33] Z. Sun and F.J.J. Schrijer and F.S.B.W. van Oudheusden. *The three dimensional flow organization past*

a micro-ramp in a supersonic boundary layer. Physics of Fluids, 2012.

[34] B. Konig and M. Patzold and T. Lutz and E. Kramer and H. Rosemann. *Numerical and experimental validation of three dimensional shock control bumps.* Journal of Aircraft, 46(2):675-682, 2009.

[35] O. Marxen and U. Rist. *Mean Flow Deformation in a Laminar Separation Bubble: Separation and Stability Characteristics.* Journal of Fluid Mechanics, 660:37-54, 2010.

[36] A. J. Smits and J. P. Dussauge. Turbulent Shear Layers in Supersonic Flow: 2nd ed, Springer Verlag, New York, 2006.

[37] J. P. Boris and F. F. Grinstein and E. S Oran and R. J. Kolbe. *New insights into large eddy simulation.* J. Fluid Dyn. Res, 10:199-228, 1992.

[38] C. Fureby and F. F. Grinstein. *Monotonically Integrated Large Eddy Simulation of Free Shear Flows.* AIAA J., 37(5):544-556, 1999.

[39] C. Fureby and F. F. Grinstein. *Large Eddy Simulation of High-Reynolds-Number and wall-Bounded Flows.* J. Comput. Phys., 181:68-97, 2002.

[40] F. F. Grinstein and L. G. and W. J. Rider. Implicit Large Eddy Simulation. Cambridge university press, 2007.

[41] M. R. Visbal and P. E. Morgan and D. P. Rizzetta. *An Implicit LES Approach Based on High-Order Compact Differencing and Filtering Scheme.* AIAA paper 2003-4098, 2003.

[42] P. E. Morgan and D. P. Rizzetta and M. R. Visbal. *Large-Eddy Simulation of Separation Control for Flow over a Wall-Mounted Hump.* AIAA J., 45(11):2643-2660, 2007.

[43] D. P. Rizzetta and M. R. Visbal and D. Gaitonde. *Large-Eddy Simulation of the Supersonic Compression-Ramp Flow by High-Order Method.* AIAA J., 39(12):2283-2292, 2001.

[44] D. P. Rizzetta and M. R. Visbal. *Application of Large-Eddy Simulation to Supersonic Compression Ramps.* AIAA J., 40(8):1574-1581, 2002.

[45] E. Garnier. *On the Use of Shock-Capturing Schemes for Large-Eddy Simulation.* J. Comput. Phys., 153:272-311, 1999.

[46] F. Ladeinde and X. Cai and M. R. Visbal and D. V. Gaitonde. *Turbulent spectra characteristics of high order schemes for direct and large eddy simulation.* Applied Num. Math, 36:447-474, 2001.

[47] R. Gao and J. Yu and W. Kong and C. Yan. *Evaluation of a WENO Method in Implicit Large Eddy Simulation of Circular Cylinder Flow.* The 2nd International Conference on Computer and Automation Engineering (ICCAE), 2010.

[48] Q. Li and C. Liu. *LES for Supersonic Ramp Control Flow Using MVG at M=2.5 and Req=1440.* AIAA J., AIAA 2010-0592, 2010.

[49] R. Mohd and Z. Hossein and C. I. Azam and K. Konstantinos. *Micro-Ramps for Hypersonic Flow Control.* Micromachines, 3(2):364-378, 2012.

[50] Q. Li and C. Liu. *Numerical Investigations on the Effects of the Declining angle of the trailing-edge of MVG.* AIAA Paper 2010-714, 2010.

[51] C. Liu and L. Chen. *Study of Mechanism of Ring-Like Vortex Formation in Late Flow Transition.* AIAA Paper 2010-1456, 2010.

[52] F. Lu and A. Pierce and Y. Shih. *Experimental study of near wake of micro vortex generators in supersonic flow.* AIAA Paper 2010-4623, 2010.

[53] Z. Sun and F.F.J. Schrijer and F. Scarano and B.W.V. Oudheusden. *PIV Investigation of the 3D Instantaneous Flow Organization behind a Micro-Ramp in a Supersonic Boundary Layer.* University of Delft, ISSW28, Manchester, UK, July 17-22, 2011.

[54] H. A. Hollingsworth & Richards. *A schlieren study of the interaction between a vortex and a shock wave in a shock tube.* AIAA J. Aeronaut. Res. Counc. Rep., 1995.

[55] D. S. Dosanjh and T. M. Weeks. *Interaction of a starting vortex as well as a vortex street with a traveling shock wave.* AIAA J., 3:216-223, 1965.

[56] O. Inoue and Y. Hattori. *Sound generation by shock-vortex interactions.* J. Fluid Mech., 380:81-116, 1999.

[57] F. Grasso and S. Pirozzoli. *Shock-Wave-Vortex Interactions: Shock and Vortex Deformation, and Sound Production.* Theoret. Comput. Fluid Dynamics, 13:421-456, 2000.

[58] M. Piller and E. Stalio. *Compact finite volume schemes on boundary-fitted grids.* Journal of Computational physics, 227:4726-4762, 2008.